PCCP

RSC Publishing

PAPER

Hydrogen adsorption and desorption at the Pt(110)-(1 × 2) surface: experimental and theoretical study

Cite this: DOI: 10.1039/c3cp44503h

Sigrídur Gudmundsdóttir,[a] Egill Skúlason,[a] Kees-Jan Weststrate,[b] Ludo Juurlink[b] and Hannes Jónsson*[a]

The interaction of hydrogen with the Pt(110)-(1 × 2) surface is studied using temperature programmed desorption (TPD) measurements and density functional theory (DFT) calculations. The ridges in this surface resemble edges between micro-facets of Pt nano-particle catalysts used for hydrogen evolution (HER) and hydrogen oxidation reactions (HOR). The binding energy and activation energy for desorption are found to depend strongly on hydrogen coverage. At low coverage, the strongest binding sites are found to be the low coordination bridge sites at the edge and this is shown to agree well with the He-atom interaction and work function change which have been reported previously. At higher hydrogen coverage, the higher coordination sites on the micro-facet and in the trough get populated. The simulated TPD spectra based on the DFT results are in close agreement with our experimental spectra and provide microscopic interpretation of the three measured peaks. The lowest temperature peak obtained from the surface with highest hydrogen coverage does not correspond to desorption directly from the weakest binding sites, the trough sites, but is due to desorption from the ridge sites, followed by subsequent, thermally activated rearrangement of the H-adatoms. The reason is low catalytic activity of the Pt-atoms at the trough sites and large reduction in the binding energy at the ridge sites at high coverage. The intermediate temperature peak corresponds to desorption from the micro-facet. The highest temperature peak again corresponds to desorption from the ridge sites, giving rise to a re-entrant mechanism for the thermal desorption.

Received 13th December 2012,
Accepted 5th March 2013

DOI: 10.1039/c3cp44503h

www.rsc.org/pccp

I. Introduction

The interaction of hydrogen with the surface of platinum metal is of fundamental importance to a wide range of technologies including various catalytic reactions, electrolysis and hydrogen fuel cells. The metal is typically dispersed in small particles embedded in a matrix. The trend is to make the particles smaller, even down to the nanoscale. For particles of FCC metals, the most common facets will be the low energy (111) and (100) facets.[1] It has been suggested that the catalytically active sites are steps on these facets[2] or edges between the facets.[3] The missing row reconstructed Pt(110)-(1 × 2) surface can be used as a periodic model of edge sites between (111) facets in theoretical calculations.[4,5]

The hydrogen evolution reaction (HER) and hydrogen oxidation reaction (HOR) are the key reactions in electrolysis of water and in hydrogen fuel cells. There, solvated protons in the electrolyte and electrons from the electrode form hydrogen molecules or the molecule dissociates into protons and electrons, respectively. Simulations have been used to model the interface between the electrolyte and the electrode with density functional theory.[6–10] Minimum energy path calculations for the transitions have shown that the Tafel reaction ($2H^* <-> H_2$) is faster than the Heyrovsky reaction ($H^+ + e^- + H^* <-> H_2$) at $U = 0$ V *vs.* SHE on all transition metal surfaces, for all the common facets, with and without defects.[8] As a result, it is not necessary to include the complicated electrochemical interface in calculations of the rate of HER and HOR for these conditions, it is sufficient to focus on the formation of H_2 from adsorbed H-adatoms and dissociation of H_2 to form two H-adatoms.

The (110) surface of platinum has a missing row reconstruction, both the clean surface and the hydrogen covered surface.[11,12] The interaction of hydrogen with this surface has been studied extensively both experimentally and theoretically.[8,13–18] Engstrom *et al.*[16] carried out temperature programmed desorption (TPD), LEED and work function measurements. Their two peak TPD spectra indicated two types of binding sites

[a] *Science Institute and Faculty of Physical Sciences, VR-III, University of Iceland, 107 Reykjavík, Iceland*
[b] *Leiden Institute of Chemistry, Leiden University, P.O. Box 9502, 2300 RA Leiden, The Netherlands*

on the surface with desorption from the high temperature state, β_2, described by first order Langmuir kinetics consistent with attractive interaction between H-adatoms while desorption from the lower temperature state, β_1, described by second order kinetics. The ratio between the integrated desorption corresponding to the two peaks, $\beta_2:\beta_1$, was reported as 1 : 2. Consistent with the general trend for H-adatoms to prefer high coordination sites on metal surfaces, this was interpreted in terms of preferential binding to the trough sites with subsequent binding to facet sites. A third peak in the TPD spectrum, labeled α, with integrated desorption similar to β_2 has since been identified after longer exposure to hydrogen gas.[17]

The assignment of the three peaks in the TPD to binding sites on the surface has remained controversial. He-atom scattering experiments indicated that H-atoms first fill sites associated with the edge since a large increase in corrugation of the He–surface interaction potential was observed upon low coverage adsorption of hydrogen.[19] This, however, remained controversial[18] and preference for trough sites continued to be widely assumed. Results of DFT calculations have since shown clear preference for the low coordinated ridge sites.[13,15] The trough sites have the weakest binding, weaker than sites on the (111) micro facets. It is tempting to assign the three peaks in the TPD spectra to three binding sites on the surface: the bridge site on the ridge (β_2), the on-top site on the facet (β_1) and the long bridge site in the trough (α), see Minca *et al.*[13] The binding energy and coverage ratio between these binding sites match qualitatively the order of the TPD peaks and the integrated desorption for each peak. But, unlike direct desorption of atoms and intact molecules from surfaces, associative desorption can involve an activation energy barrier and the interpretation of TPD spectra is, therefore, not straightforward.

Previous theoretical calculations of hydrogen on Pt surfaces have mostly focused on the binding energy at various sites and the construction of potential energy surfaces for dynamical calculations of the dissociative adsorption on clean Pt surfaces. Here, we report results of calculations of the activation barrier for hydrogen desorption and adsorption at the Pt(110)-(1 × 2) surface as a function of coverage, ranging from zero to full coverage. Calculations of H-binding to the Pd(110)-(1 × 2) surface are also presented for comparison. In addition, we report measured TPD spectra of H_2 desorption from the Pt(110)-(1 × 2) surface which has been designed to avoid H_2 desorption from edges of the crystal, which can introduce other sites than those under investigation. With this setup, a high temperature shoulder-free spectrum is observed. We give a new interpretation of the experimental TPD spectra for the Pt(110)-(1 × 2) surface (preliminary description of the simulation results has been reported in ref. 20). The activation energy barriers obtained from the DFT calculations are used to simulate TPD spectra using coupled kinetic equations and the results show that the common way of assigning each peak in a TPD spectrum to a different binding site on the surface does not accurately represent the mechanism of the associative desorption process on this surface. Here, we give the more complete description of the calculations and present new experimental measurements of the TPD spectrum.

II. Methodology

The density functional theory (DFT)[21] calculations for the structure relaxations and minimum energy path (MEP) calculations were performed using the Vienna *ab initio* Simulation Package (VASP)[22] using the RPBE functional approximation.[23] The d-band center calculations were performed using the Dacapo software[24] with the same RPBE functional. In each case, the optimized lattice constant was used, 4.011 Å in VASP and 4.020 Å in Dacapo. All calculations used a plane-wave basis to represent valence electrons and ultra-soft pseudopotentials[25,26] to represent the ionic cores. A plane wave cutoff of 33 Ry (450 eV) was used in the VASP calculations and 26 Ry (354 eV) in the Dacapo calculations. Only insignificant differences were found between results obtained from the two software packages.

The Pt(110)-(1 × 2) system as well as the Pd(110)-(1 × 2) system consist of most of the calculations of an eight layer thick periodic (3 × 2) model cell with one row of the top layer missing. The bottom four layers were kept frozen while the upper four layers were allowed to relax. The RPBE optimized lattice constant for Pt was also used for the Pd surface calculations. A k-point sampling of the 4 × 4 × 1 Monkhorst–Pack grid was used in all calculations. The spacing between periodic images of the slabs was at least 10 Å. All configurations were optimized until atomic forces were less than 0.01 eV $Å^{-1}$. Convergence tests for the k-point sampling were performed for the Pt(110)-(1 × 2) where a comparison of 4 × 4 × 1 and 6 × 6 × 1 k-point sampling gave in all cases an energy difference of less than 0.01 eV.

The minimum energy paths (MEPs) for diffusion and adsorption–desorption of hydrogen were calculated using the climbing image nudged elastic band (CI-NEB) method.[27–29] The activation energy was calculated from the MEPs and rates estimated using harmonic transition state theory. The work function was calculated as the difference between the electrostatic potential in the central, vacuum region and the Fermi level. The exchange–correlation potential was excluded from the potential since it decays rather slowly in the vacuum region but necessarily should go to zero in the vacuum where the charge density goes to zero.

A home-built surface science system in Leiden was used to experimentally study H_2 desorption from the clean Pt(110)-(1 × 2) surface. The system is equipped with a sputter ion gun for sample cleaning, LEED optics (VG RVL900), and a differentially pumped quadrupole mass spectrometer (QMS, UTI 100c). The base pressure is lower than 5×10^{-10} mbar. The sample is a 6 mm diameter and 1 mm thick Pt sample cut and polished to expose a (110) plane (by Surface Preparation Laboratories, Zaandam, The Netherlands). The sample is cooled through contact with a liquid N_2 cryostat and heated resistively using electrical current passing through the sample. The temperature is measured using a K-type thermocouple spot welded to the crystal's edge. The thermocouple is connected to a PID controller with an internal temperature reference (Eurotherm type 2416). The crystal was cleaned using repeated 2 kV Ar^+ sputtering and annealing cycles (1200 K) and LEED used to verify surface order. The absence of residual carbon was

checked by adsorbing O_2 and verifying that no CO or CO_2 appeared in temperature-programmed desorption (TPD). For TPD measurements, the sample was placed in front of a 2 mm diameter hole at a distance of 2 mm of the differentially pumped QMS. Using this approach, TPD measurements are mostly unaffected by desorption from heating wires and edges of the sample. Exposures are reported in Langmuir ($L = 1.3 \times 10^{-6}$ mbar s) and are based upon the pressure as measured by an uncalibrated nude ion gauge. The ramp rate for the TPD measurements was 3 K s^{-1}.

III. Results

A. Adsorption sites

The energy associated with the various binding sites on the surface is strongly dependent on the H-atom coverage. By adding the H-atoms to the surface one at a time, filling first the strongest binding sites and ending with the weakest ones, the energy per adatom can be calculated from the differential adsorption energy

$$\Delta E_H(n) = E(n) - E(n-1) - \frac{1}{2}E_{H_2} \quad (1)$$

where n is the number of hydrogen atoms adsorbed on the surface and $E(n)$ is the total energy of the surface with n atoms adsorbed. The results are shown in Fig. 1. The hydrogen coverage, θ_H, is defined as the ratio of the number of H-adatoms to the number of surface Pt-atoms, $\theta_H = n/N_{surf}$.

In an agreement with the results of Zhang *et al.*,[13,15] we find that the short bridge site on the ridge (R) is the strongest adsorption site at low coverage. The hydrogen adsorption energy on the ridge was calculated to be −0.28 eV H^{-1} while the adsorption energy at the FCC threefold hollow site of the (111) micro facet and the long bridge in the trough were −0.23 eV H^{-1} and −0.06 eV H^{-1}, respectively. Table 1 shows the binding energy for all adsorption sites considered and Fig. 1 shows the adsorption sites. When the ridge has been filled, the preferred sites are the tilted on-top sites on the micro facets (F) followed by adsorption onto the long bridge sites in the trough (T). The filling of the trough sites forces the neighboring H-atoms to move from the on-top sites towards the HCP threefold hollow sites on the (111) micro facet (F′).

Table 1 Binding energy of a single H-adatom on Pt(110)-(1 × 2) and Pd(110)-(1 × 2) on various surface sites, and at higher coverage for ridge sites where R, R2, and R3 indicate 1/3, 2/3, and 3/3 filling of the sites

Sites	ΔE_H Pt(110) (eV)	ΔE_H Pd(110) (eV)
R	−0.28	−0.22
R2	−0.34	−0.18
R3	−0.40	−0.16
F	−0.21	—
F′	−0.14	−0.28
FCC	−0.23	−0.36

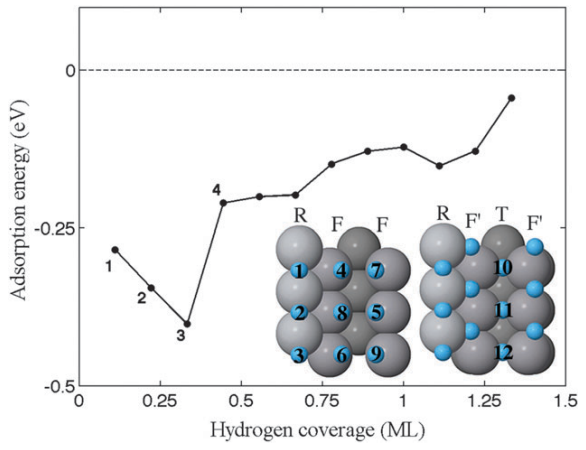

Fig. 1 Differential H-atom adsorption energy as a function of hydrogen coverage for the Pt(110)-(1 × 2) surface. The insets show the adsorption sites and the order in which they get filled, first short bridge on the ridge (R), then tilted on-top on the micro facet (F), and finally the HCP hollow site (F′) and the long bridge site in the trough (T). A strong attraction can be seen between the H-adatoms on the ridge, while there is a weak repulsion on the micro facets and a stronger repulsion in the trough.

As mentioned in the Introduction, it has frequently been assumed that the strongest adsorption site on the Pt(110)-(1 × 2) surface is the highly coordinated trough sites[16,18] or the three-fold hollow sites of the (111) micro facet,[17,30] but the DFT calculations give strongest binding at the ridge sites. In order to test this prediction of the DFT calculations, we compare the calculated work function as a function of coverage and He–surface interaction with previously reported experimental measurements.

1. Work function change. Engstrom *et al.*[16] reported measurements of the change in work function, $\Delta\phi$, with hydrogen coverage. An initial rise in the work function occurred up to 1/3 of relative coverage followed by a decrease with further adsorption of hydrogen, as shown in Fig. 2. Later, Shern[18] reported work function measurements obtained by MEM-LEED showing the same trend and interpreted this to indicate adsorption in trough sites. The DFT calculated work function change as H-atoms are added to the ridge sites, however, reproduces the initial rise measured by Engstrom *et al.* and Shern, followed by a decrease when hydrogen atoms are added to the facet sites, as shown in Fig. 2. The magnitude of the work function can, however, be quite sensitive to the functional used[9] and the agreement here is only qualitative. The calculated work function for the clean Pt(110)-(1 × 2) surface is 0.4 eV smaller than that of the flat Pt(111) surface. Based on the jellium model, the Pt(110)-(1 × 2) surface can be expected to form a surface dipole with the ridge Pt atoms being electron deficient because of the tendency to smooth out the electron density, the Smoluchowski effect.[31] The surface dipole formed on the Pt(110)-(1 × 2) surface then decreases the work function compared to that of the flat Pt(111) surface. Hydrogen atoms bound to the surface have a slightly negative charge, *ca.* −0.05 e, as determined by Bader analysis,[32,33] so a hydrogen adatom on top of the ridge decreases the surface dipole and increases the work function towards that of the flat surface. The facet sites are positioned lower and have the opposite effect. Similar site dependence of

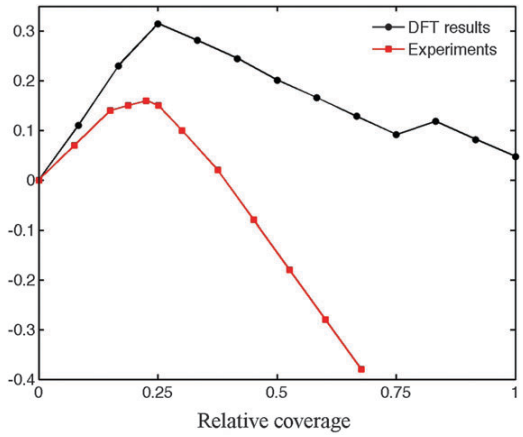

Fig. 2 Calculated (circles) and measured (squares)[16] work function change *vs.* relative coverage of hydrogen on Pt(110)-(1 × 2). The work function of a clean surface is used as a reference state. The work function initially increases as hydrogen atoms adsorb onto the ridge because the slightly negative H-adatoms (with a charge of −0.05 e) partly cancel the positive charge at the ridge arising from the Smoluchowski effect, thereby increasing the work function towards that of the flat Pt(111) surface. Adsorption on the lower facet sites, however, leads to a decrease in the work function.

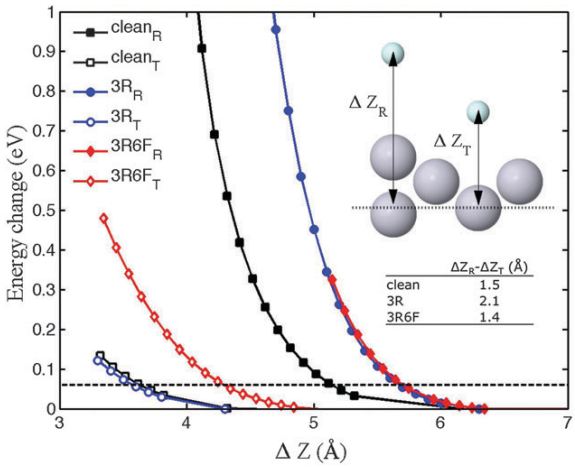

Fig. 3 Interaction energy of a He-atom with the Pt(110)-(1 × 2) surface, clean (squares) and with H-atoms in the ridge sites (circles) and with H-atoms in both ridge and facet sites (diamonds). Filled symbols correspond to He-atoms approaching the surface above a ridge site, while open symbols correspond to an approach above a trough site. The inset shows a side view of the surface and the two approach directions. The inset table shows the calculated corrugation amplitude corresponding to 60 meV for the three configurations. The agreement with the experimental He scattering results is excellent, verifying the site preference predicted by the DFT calculations.

the effect of adsorbates on work function has been reported by Leung *et al.* in studies of metal atom adsorption on tungsten surfaces.[34]

2. He–surface interaction. He-atom diffraction from H/Pt(110)-(2 × 1) was measured by Kirsten *et al.*[19] and analyzed to obtain the corrugation of the He–surface interaction potential as a function of H-atom coverage. The results showed strong variation, the corrugation increasing from 1.5 Å for a clean surface to 2.0 Å after filling the β_2 state and then decreasing again to close to that of the clean surface after filling also the β_1 state. The initial increase in corrugation is a clear indication that the strongest binding sites for H-adatoms are associated with the ridge, but the exact location of the site could not be determined from the He scattering data. It was suggested that the H-atoms are located in subsurface sites under the outermost Pt ridge atoms.[19] Zhang *et al.*[15] showed by LEED measurements that the filling of subsurface sites can be ruled out because it would necessarily lead to large relaxation of the Pt atoms but none was observed. We carried out DFT calculations of a He atom at various positions above the surface and estimated the corrugation of the interaction potential corresponding to the beam energy used in the experiments, 60 meV. Fig. 3 shows the variation in the energy change when bringing a He-atom close to the surface, both directly above the ridge and directly above the trough, for a clean surface, a surface with ridge sites filled and a surface with ridge and facet sites filled. The results show the corrugation amplitude increasing from 1.5 Å to 2.1 Å when going from a clean surface to a surface with ridge sites filled, and then decreasing again down to 1.4 Å when the facet sites are filled with H-atoms. This is in excellent agreement with the measurements of Kirsten *et al.* lending strong support for the results of the DFT calculations.

It should be noted that the corrugation of the He-surface potential at 60 meV energy is quite insensitive to the dispersion interaction and can, therefore, be predicted quite well with DFT/GGA calculations even though the long range dispersion interaction is not included at that level of theory.

3. Comparison with H/Pd(110)-(1 × 2). The observed preference of the H-atoms for the low coordinated ridge site is very different from the general trend for H-adatoms to prefer high coordination sites. For comparison, we carried out some calculations of H-adsorption on the Pd(110)-(1 × 2) surface. The missing row reconstructed Pd(110) surface is only metastable when it is clean, but becomes preferred after hydrogen has been added.[12] The site preference of H-atoms is very different for Pd(110)-(1 × 2) (Table 1). The short bridge sites on the ridge (R) are not the most stable sites on the Pd(110)-(1 × 2) surface but rather the FCC three-fold hollow sites on the (111) micro-facet. Also, there is no attractive interaction between the neighboring hydrogen atoms at the ridge sites of the Pd surface as observed on the Pt surface. Instead a small repulsive interaction is found. It is clear that even though these two metals are similar in many respects, the difference in electronic structure (4d *vs.* 5d metals) leads to quite different interaction with hydrogen.

B. Associative desorption

The interpretation of TPD data typically assumes that the weakest bound atoms desorb first as the temperature is increased. However, based on our calculations of the activation energy of hydrogen associative desorption from the three different binding sites of the Pt(110)-(1 × 2) surface, shown in Fig. 4, that is not always the case. Other desorption mechanisms with hydrogen desorbing from two different types of adsorption sites were also considered but gave higher barrier than desorption from two ridges or two facet sites. The two

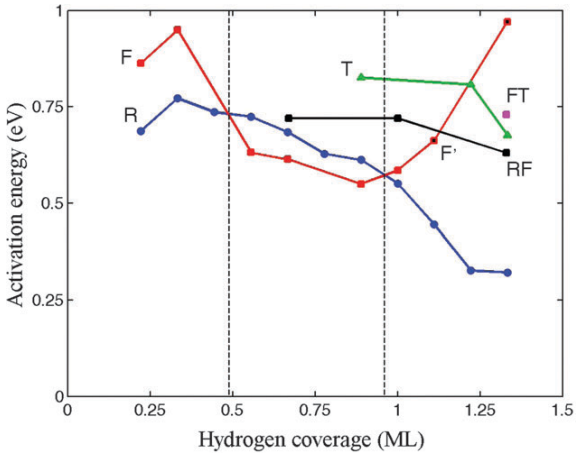

Fig. 4 Activation energy for desorption from five different pairs of sites on the surface as a function of coverage: the ridge (R, blue circles), the facet (F and F′, red squares), the trough (T, green triangles), the ridge and facet (RF, black squares) and facet and trough (FT, magenta squares) sites. The optimal desorption mechanism changes with coverage: at high coverage desorption occurs from the strong adsorption sites on the ridge, at intermediate coverage from the sites on the micro-facet and at low coverage again from the ridge sites. At high coverage, the less stable final state is kinetically preferred because of low catalytic activity of the Pt-atoms at the trough sites.

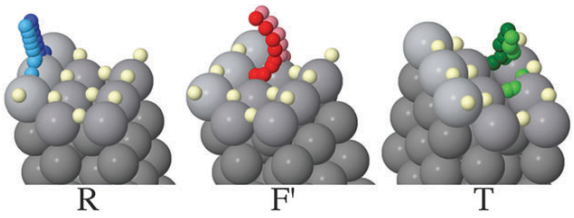

Fig. 5 Atom configurations for desorption from ridge (R, blue), (111) micro facets (F′, red) and trough (T, green) of a fully covered surface. The surrounding hydrogen atoms (base color) are only shown in their initial relaxed positions.

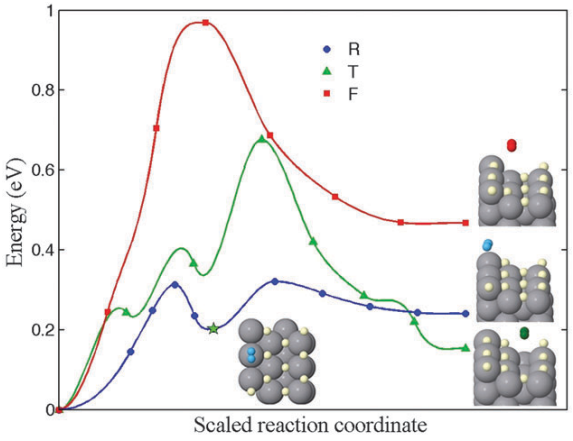

Fig. 6 A comparison of the minimum energy paths (MEPs) for the desorption from ridge (R, blue), (111) micro-facet (F′, red) and trough (T, green) sites of a fully covered surface. The configurations obtained in the NEB calculation are shown. The star indicates local minimum observed on the ridge MEPs found by a separate relaxation. It corresponds to a Kubas complex with H–H bond length of 0.89 Å at a height 1.73 Å above the ridge Pt atom (bottom inset). The final configurations for the three desorption processes are shown as insets to the right. The height of the H_2 molecule in the final configurations is more than 4 Å above the underlying Pt-atoms.

crossings of the three desorption activation energy curves split the desorption mechanism into three coverage regions. At the highest coverage, the desorption of H_2 from the weakest bound H-adatoms in the trough with total binding energy of 0.15 eV involves a high activation energy barrier of 0.68 eV, while the desorption of H_2 formed from the more strongly bound H-adatoms on the ridge, with a total binding energy of 0.24 eV, has an activation barrier of 0.32 eV. This is in apparent contradiction to the so-called Brønsted–Evans–Polanyi (BEP) principle, which says that the activation energy is linearly related to the reaction energy. The BEP principle has been shown to work well in heterogeneous catalysis when comparing processes with the same mechanism and taking place at the same type of surface sites.[35] In the present case, however, the less stable final state turns out to be kinetically preferred when comparing processes taking place at two different surface sites – ridges and troughs. This shows how important it is to evaluate the activation energy rather than just the reaction energy in order to determine the active site on a surface.

The reason the activation barrier for desorption from the weakly binding trough sites is so high is the low catalytic activity of the highly coordinated underlying Pt atoms. The MEP for the desorption from trough sites (T) is quite complicated (see Fig. 5). Surrounding H-atoms get shifted around to make room for H–H bond formation at a facet Pt-atom. The MEPs for desorption of H_2 formed from trough (T), micro-facet (F′) and the ridge (R) H-atoms at full coverage are shown in Fig. 6. Desorption at the ridge and at the trough leads to intermediate local minima on the MEP. They were found during the NEB calculation but subsequently refined by separate minimization of these configurations. For the trough desorption, these local minima are due to rearrangement of hydrogen atoms on the surface. However, the local minimum in the MEP for desorption from ridge corresponds to a Kubas complex[36] where the nearly intact H_2 molecule is bound as a ligand to a surface Pt atom. This complex is formed in the desorption from ridge sites at all coverages. The H–H bond length is about 0.9 Å, the height above the underlying Pt ridge atom 1.6–1.7 Å and binding energy 0.04–0.24 eV depending on coverage. The H_2 molecule is nearly a free rotor in the Kubas complex.

Based on the NEB calculations, the desorption mechanism first involves desorption from ridge sites, followed by desorption from facet sites as well as from ridge sites as they get refilled by diffusion from the facet and finally, at low coverage, again desorption from ridge sites. Fig. 7 shows the atom configuration along the MEPs obtained in the NEB calculations for each coverage region. It has recently been argued[37] that the Pt(110)-(1 × 2) surface is not a good model for an edge on a nano-particle but there it was assumed that the active sites on the Pt(110)-(1 × 2) surface are the trough sites. Our results show that this is not the case.

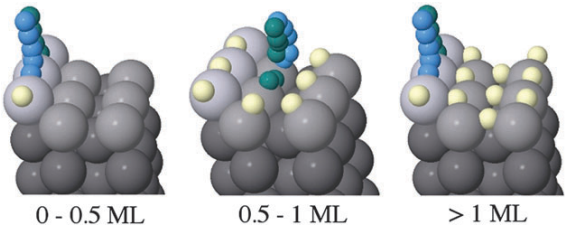

Fig. 7 Atom configurations along the MEP for the desorption mechanism with lowest activation energy in each of the three coverage intervals defined in Fig. 4: desorption from ridge sites (R) for coverage below 0.5 ML, from facet sites (F) for coverage between 0.5 and 1 ML and again desorption from ridge sites (R) at coverage above 1 ML. The surrounding hydrogen atoms (beige color) are only shown in their initial positions.

C. Surface diffusion

The question now arises how efficient the surface diffusion is in filling the ridge sites after H_2 molecules have desorbed at high coverage. Fig. 8 shows MEPs for surface diffusion where H-atoms refill the ridge sites. At high coverage, H-adatoms diffuse from the facet HCP sites (F′) to the ridge (R) and then trough adatoms (T) diffuse to the facet (F or F′). A maximum barrier of 0.25 eV is obtained for these processes. At low coverage, the diffusion is easier as the facet (F) atoms can diffuse to the ridge with a barrier of 0.1 eV. This low coverage value can be compared with the activation energy calculated for diffusion on the Pt(111) surface, 0.04 eV, using the same functional.[38] It is important to note here that refilling of the ridge sites is not a concerted process with the desorption, but rather a separate, activated process. The diffusion paths are fairly long and the NEB calculations show these intermediate local minima with activation barriers in between. However, since the rate of the diffusion processes is higher than the rate of H_2 desorption, the system will equilibrate and find the lowest energy configuration in between desorption events.

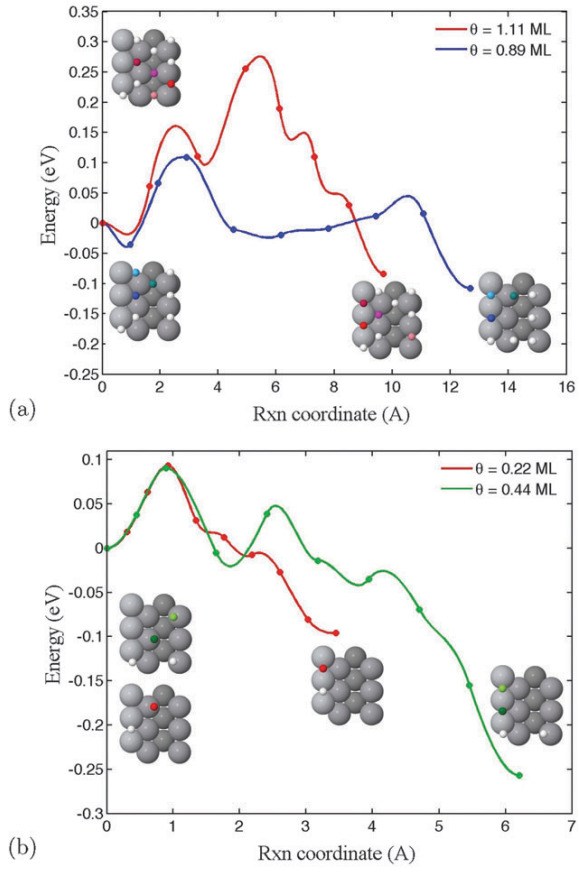

Fig. 8 Calculated minimum energy paths for H-atom diffusion toward the lowest energy configuration after desorption from ridge for (a) high coverage of 1.11 ML (red) and 0.89 ML (blue) and (b) low coverage of 0.44 ML (green) and 0.22 ML (red). High coverage includes diffusion from the HCP sites (F) to the ridge (R) and then diffusion from the trough (T) to the facet (F or F) sites while at low coverage the diffusion is from the facet (F) to the ridge (R). Insets show the initial and final configurations for each MEP.

D. TPD modeling

To simulate the TPD spectra a simple model with coupled differential equations was set up. A numerical solution of the equations giving the rate of desorption of H_2 as a function of temperature was obtained using a finite difference method. The H/Pt(110)-(1 × 2) system was described by including three types of binding sites, ridges (R), facets (F) and troughs (T). Here, the F and F′ sites are treated as the same binding site since the difference in adsorption energy is small and they cannot both be occupied at the same time. Also, once hydrogen atoms adsorb on the T sites, neighboring F atoms are pushed to F′ sites. The model includes desorption from the R and F sites as well as diffusion between the various binding sites. The attractive interactions between the neighboring hydrogen atoms on the ridge lead to first order kinetics for the desorption from the ridge. The experimentally observed shift in the β_1 peak with different initial coverage has been interpreted to indicate second order kinetics.[16] Hence, we describe desorption from facet sites with a second order rate equation. However, similar spectra are obtained when desorption from both types of sites is described with first order rate equations. The shift in the β_1 peak with coverage is then due to the strong coverage dependence of the activation energy barrier. The rate equations for hydrogen desorption are then

$$\frac{d\theta_R}{dt} = \left[-2k_{R,H_2} - k_{R,F}\right]\theta_R(t) + k_{F,R}2\theta_F(t) \quad (2)$$

$$\frac{d\theta_F}{dt} = \left[-2k_{F,H_2}\theta_F(t) - k_{F,R} - k_{F,T}\right]\theta_F(t) + k_{R,F}\frac{1}{2}\theta_R(t) + k_{T,F}\frac{1}{2}\theta_T(t) \quad (3)$$

$$\frac{d\theta_T}{dt} = -k_{T,F}\theta_T(t) + k_{F,T}2\theta_F(t). \quad (4)$$

Here, θ_i is the coverage of H-adatoms at binding sites of type i and the factors 2 and 1/2 in front of θ come from the number of adsorption sites of each type. $k_{X,Y}$ is the rate constant for transition from initial state X to final state Y given by the

Table 2 Constants for the polynomial fits of E_a^R and E_a^F used in the TPD simulation

R	a_i^R	b_i^R	c_i^R
C^R		0.6738	
1	0.5646	0.8842	−0.2641
2	−1.6071	4.1527	−0.5135
3	—	−12.703	3.8956
4	—	11.853	—
F	a_i^F	b_i^F	c_i^F
C^F		0.9361	
1	1.3923	−1.1024	0.6156
2	−22.746	9.7425	−20.125
3	50.37	−57.51	242.26
4	—	176.58	−586.37
5	—	−269.53	—
6	—	162.03	—

Arrhenius equation with pre-exponential ν and activation energy E_a

$$k(\tau,\theta_R,\theta_F,\theta_T) = \nu\, e^{-E_a(\theta_R,\theta_F,\theta_T)/k_B\tau}. \quad (5)$$

The total desorption rate per surface site is then

$$r(\tau,t) = k_{R,H_2}(\tau)\theta_R(t) + 2k_{F,H_2}(\tau)\theta_F(t). \quad (6)$$

To simulate our TPD experiment we set $\tau = \tau_0 + \alpha t$ where τ_0 = 135 K is the initial temperature and α = 3 K s^{-1} the heating rate.

A polynomial fit to the calculated activation energy curves in Fig. 4 for ridge and facet desorption was made taking into account interaction with the various types of neighbors,

$$E_a(\theta_R,\theta_F,\theta_T) = C + \sum_i a_i\theta_R^i + \sum_i b_i\theta_F^i + \sum_i c_i\theta_T^i \quad (7)$$

where θ is the hydrogen coverage at the various binding sites, and the constants C, a_i, b_i and c_i C^R, C^F, a_i, b_i and c_i have different values for the two desorption sites, F and R, see Table 2.

The polynomial fit used for the TPD simulation represents the DFT calculated activation energy to within ±0.1 eV in the important regions, as can be seen in Fig. 9. The activation energy for diffusion between adsorption sites was taken from the NEB calculations discussed above. Diffusion is in all cases much faster than desorption. This difference in time scale led to inefficiencies in the numerical integration of the kinetic equations. In order to speed up the simulation, the diffusion barriers were increased to allow for a larger time step in the finite difference calculations. Based on the lowest desorption activation energy at each time, care was taken that the diffusion was always significantly faster than the desorption and that detailed balance between sites was maintained. The results were independent of the choice of diffusion barriers as long as the system was able to reach optimal configuration of the adsorbate for each coverage.

Engstrom *et al.*[16] determined the prefactor for hydrogen desorption from the temperature dependence of the TPD spectra and obtained a value of 10^{11} s^{-1}. The formation of the Kubas complex makes the calculation of the prefactor and application of harmonic transition state theory questionable and we have chosen to adopt the experimental value rather than to calculate it by DFT.

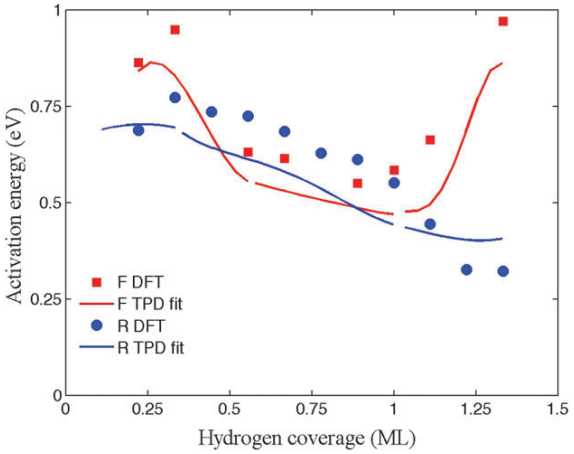

Fig. 9 A comparison of the polynomial fit of the desorption activation energy used in the TPD simulation and the DFT results for the ridge (R, blue circles) and facet (F or F′, red squares) desorption. The fit agrees with the DFT value to within 0.1 eV, which is a typical estimate of an error bar in DFT calculations.

1. Experimental TPD. Fig. 10 shows our experimental series of TPD measurements as solid lines ranging between estimated doses of 1 and 1000 L. With increasing hydrogen exposures, we observe the subsequent development of the previously reported β_2, β_1 and α peaks.[11,13,16,17] We also observe the α^* peak reported by Anger *et al.*[17] (dotted line) for all larger exposures ranging up to 10 000 L. This peak has been attributed to H_2O desorption from the hydrogen-covered sample that was detected as the H_2^+ cracking fragment. In line with this interpretation and consistent with general observations of H_2O desorption from hydrogenated Pt nanostructured surfaces,[39,40] we even observe water desorption from a second water layer for very long H_2 exposures (indicated as the α^{**} peak).

In comparison to previous TPD studies, we find very good agreement with the data presented by Minca *et al.*[13] Peak positions for β_2 (302 K) and α (185 K) are the same to within 1 K. Anger *et al.*[17] reported a slightly lower maximum desorption temperature for β_2 (295 K *vs.* 302 K) but the same for the α peak. Relative intensities of the peaks also compare well. As we have previously found that Gaussian line shapes provide reasonable fits to H_2 TPD traces for comparable nanostructured Pt surfaces,[41] we crudely estimate the area belonging to the various peaks in Fig. 10 by fitting Gaussian line shapes to the α and β_2 peaks. The remainder is considered to belong to the β_1 peak. The relative integrals are thus roughly estimated to be 1.1 : 1.8 : 1.0 for the α, β_1, and β_2 peaks, respectively. Our procedure is different from that of Minca *et al.*,[13] but agrees within experimental error with the 1 : 2 : 1 ratio. The only significant difference between our measurements and the data reported by Minca *et al.* is the shoulder on the high temperature side of the β_2 peak around 350 K. Use of a differentially pumped QMS ensures that both our and Anger *et al.* studies are sensitive only to H_2 desorption from the front surface. In our

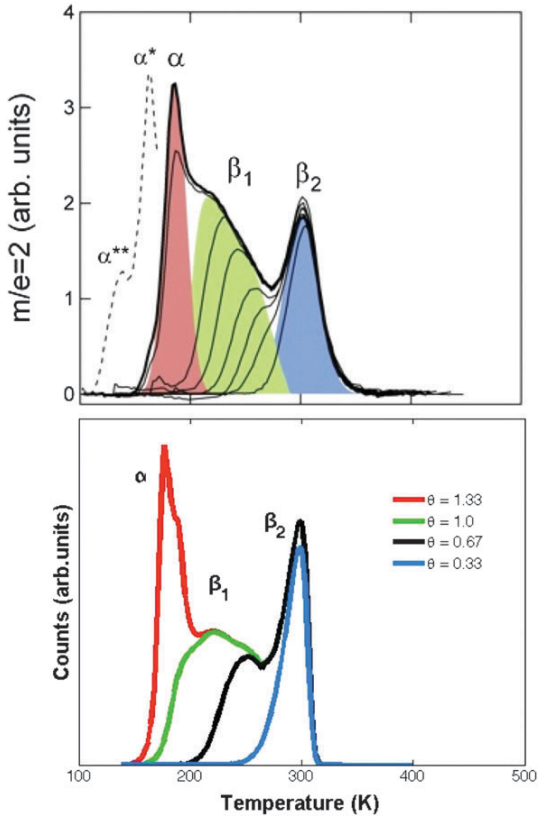

Fig. 10 Top half: experimental TPD spectra for various doses of hydrogen (solid lines, estimated from 1 to 1000 L) and fitted Gaussian line shapes (colored areas) for the α and β_2 peaks, with remainder associated with the β_1 peaks. The dashed line shows the initial TPD trace of a 5000 L dose, likely contaminated by H_2O. Bottom half: simulated TPD spectra based on the DFT results and finite difference solution of the coupled rate equations for relative initial coverage of 1.33 (red), 1.0 (green), 0.67 (black) and 0.33 (blue).

data, there is no high temperature shoulder. Desorption at 350 K is characteristic of the (100) step type on Pt surfaces.[40] In the study by Minca *et al.* the high temperature shoulder may, therefore, be caused by desorption from the crystal's edge which is orthogonal to the (110) surface and likely contains a high number of such steps.

2. Simulated TPD. Fig. 10 (bottom half) shows the simulated TPD spectra for four different values of the initial coverage. The initial configuration for a given coverage was chosen to be the lowest energy configuration, filling the ridge sites first (up to 0.33 ML), then the facet sites (0.33–1 ML) and finally the trough sites (1–1.33 ML). The simulation agrees well with the measurements, showing three peaks when starting with full coverage, θ = 1.33 ML, even though desorption only occurs from two types of sites, ridges and facets. At low temperature, a peak is reproduced quantitatively by desorption from the strongly bound ridge sites, rather than the trough sites where the binding energy is lowest. The β_1 peak is not only due to desorption from facet sites[11,13,16–18] but also to some extent from the ridge sites. When starting with hydrogen coverage of θ = 1.0 ML, the β_1 peak is the lowest temperature peak since, although hydrogen atoms are present at the ridge sites, the desorption energy barrier is greater than for desorption from the facet sites at this coverage. Irrespective of whether the facet desorption is modeled by first order or second order rate equations, the simulation still shows a strong shift in the position of the second peak with coverage due to the coverage dependence of the desorption activation energy. This can be seen clearly by comparing the curves for initial coverage of θ = 1.0 ML and θ = 0.67 ML. Finally, the highest temperature peak, β_2, is due to desorption from the ridge again, the same sites as the lowest temperature α peak. In agreement with our experimental data, no shoulder is obtained on the high temperature side of the β_2 peak.

E. Coverage dependence of the binding energy at ridge sites. Fig. 4 shows the large coverage dependence of the activation energy for desorption from ridge sites, starting at 0.7 eV at low coverage and dropping down to 0.32 eV at high coverage. This trend is mainly due to the change in binding energy (Fig. 11) while the energy of the saddle point is rather constant. The barrier for dissociative adsorption of a gas molecule on the ridge is only 0.03–0.1 eV at any coverage. As mentioned earlier, there are attractive interactions between neighboring hydrogen atoms on the ridge but the next nearest neighbors on the (111) micro facet cause repulsive interaction that lowers the binding energy as can be seen in Fig. 12. However, an interesting effect of the next nearest neighbors in the trough on the binding energy at the ridge sites is found in the DFT calculations. One trough neighbor lowers the binding energy more than a facet neighbor which is closer. The effect of the neighbors on the facet correlates well with the shifts in the d-band center of the ridge Pt atoms with added neighbors (Fig. 13). With added neighbors to F′, the d-band

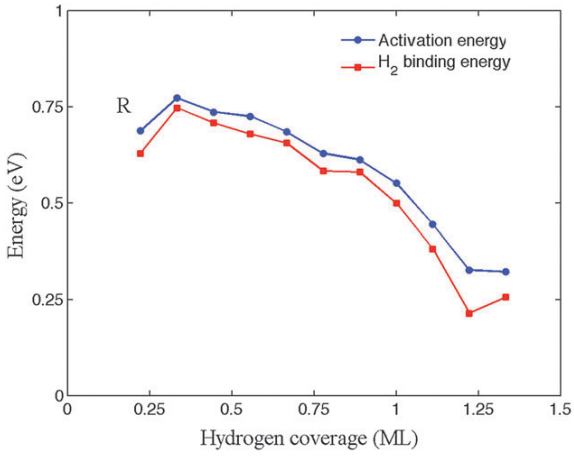

Fig. 11 Activation energy for desorption of H_2 molecules formed from H-atoms at ridge sites (blue circles) and the binding energy of two hydrogen atoms (red squares) on ridge sites as a function of coverage. The variation of the activation energy with coverage follows closely that of the binding energy. The saddle point energy is only 0.03–0.1 eV higher than the energy of a H_2 gas molecule at all coverages and does not contribute significantly to the coverage dependence of the desorption barrier.

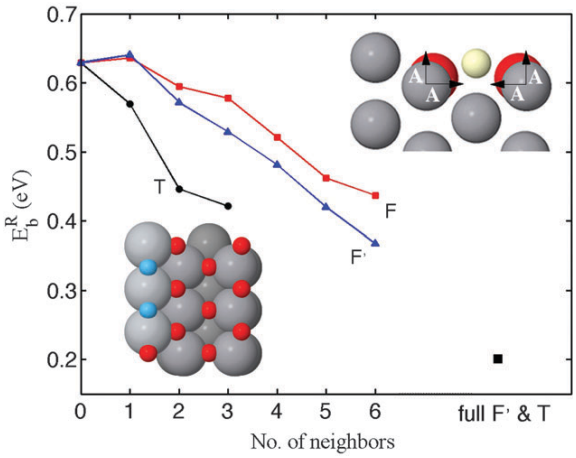

Fig. 12 Binding energy of two H-atoms at ridge sites as a function of the number of neighbors of various types: trough (T – black circles) and facet (F – red squares or F′ – blue triangles). The large black square shows the binding at full coverage where all facet (F′) and trough (T) sites are occupied.

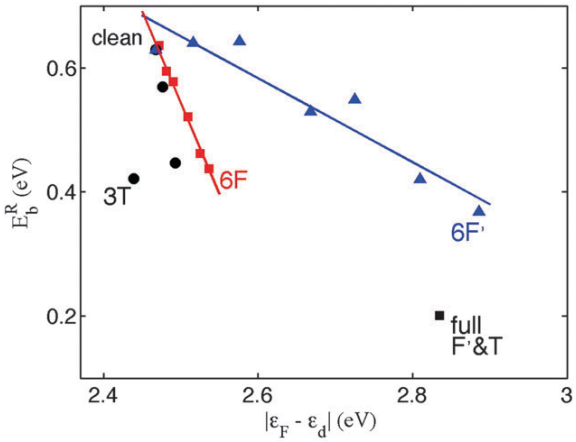

Fig. 13 Binding energy of two H-atoms at ridge sites *vs.* energy of the center of the d-band with respect to the Fermi level for various different configurations of H-atom neighbors: facet (F, red squares and F′, blue triangles) and trough (T, black circles). The large black square corresponds to a fully covered surface. The effect of F′ neighbors scales with the d-band center, but not the effect of T and F neighbors.

center moves further down from the Fermi level and the binding energy decreases. This is consistent with the d-band model.[42] Such a trend is not observed, however, for the distant neighbors in F and T sites. But, an H-atom sitting in a T or F site causes a large relaxation of the Pt atoms in the micro facet which move up and towards the trough by 0.25 Å or 0.1 Å, respectively, in each direction, as shown in the inset of Fig. 12. This flattens the surface around the ridge atoms and makes them less exposed to the hydrogen atoms, apparently thereby decreasing the binding energy to the H-atoms at the ridge. In summary, the effect of the F′ neighbors seems to be mainly due to the electronic effect while the effect of the T and F atoms is apparently correlated with surface relaxation effects.

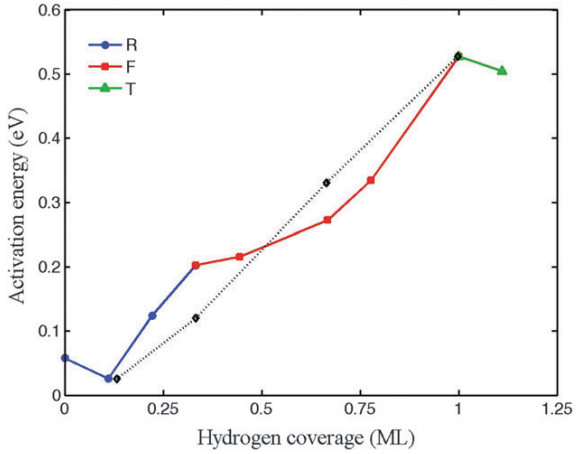

Fig. 14 Activation energy of direct adsorption as a function of hydrogen coverage. The initial adsorption is onto the short bridge on the ridge (R, blue), followed by adsorption on the facet (F, red) and finally to the long bridge site in the trough (T, green).

F. Direct adsorption

The calculated minimum energy paths (MEPs) can also be used to estimate the activation energy for dissociative adsorption of H_2 molecules on the surface at the various sites. This is shown in Fig. 14. At low coverage, adsorption onto the ridge (R) only involves small activation energy ($\approx$0.1 eV) while larger activation energy is found for adsorption onto the facet sites (F, 0.2–0.5 eV). Adsorption on the trough sites (T) involves large activation energy of 0.5 eV, reflecting the small catalytic activity of the highly coordinated Pt-atoms in the trough. These results compare well with experimental exposure curves,[13,16] as shown in Fig. 14, and are consistent with the fact that the high exposure of 10^4 L is needed to reach full coverage. We note that the system is not in equilibrium in the two experiments (adsorption by dosing and TPD) and hence detailed balance does not hold. The H_2 desorption in TPD has a reentrant mechanism of R–F–R whereas the adsorption follows the direct mechanism of R–F–T.

IV. Summary

A combined theoretical and experimental study of hydrogen interaction with the Pt(110)-(1 × 2) surface is presented where the focus is on transition mechanisms and activation barriers. The results point to possible complexities in the interpretation TPD spectra where associative desorption is governed by the activation energy rather than the binding energy and strong coverage dependence can lead to more than one peak in the TPD corresponding to desorption at a given type of surface sites. In the present case, the lowest and highest temperature peaks in the TPD both correspond to desorption from the ridge sites while the intermediate temperature peak is due to desorption from facet sites. The Pt(110)-(1 × 2) surface shows large coverage dependence of desorption activation energy and lateral attractive interaction between neighboring hydrogen atoms on the ridge. For both these features, surface relaxation

plays an important role making it necessary to allow the first few surface layers to relax when calculating the interaction of hydrogen with the surface. The results presented here can shed light on the interaction of hydrogen with Pt nanoclusters since the ridges on the missing row surface mimic edges between (111) microfacets.

Acknowledgements

We thank Jean-Claude Berthet for help with the TPD modeling. This work was funded in part by the Eimskip Fund of the University of Iceland and the Icelandic Research Fund.

References

1 C. R. Henry, *Surf. Sci. Rep.*, 1998, **31**, 231.
2 S. Dahl, A. Logadóttir, R. C. Egeberg, J. H. Larsen, I. Chorkendorff, E. Törnqvist and J. K. Nørskov, *Phys. Rev. Lett.*, 1999, **83**, 1814.
3 B. Hvolbaek, T. V. W. Janssens, B. C. Clausen, H. Falsig, C. H. Christensen and J. K. Nørskov, *Nano Today*, 2007, **2**, 14.
4 S. Gudmundsdóttir, W. Tang, G. Henkelman, H. Jónsson and E. Skúlason, *J. Chem. Phys.*, 2012, **137**, 164705.
5 E. Skúlason, A. A. Faraj, L. Kristinsdóttir, J. Hussain, S. Gudmundsdóttir and H. Jónsson, *Top. Catal.*, 2013.
6 E. Skúlason, G. S. Karlberg, J. Rossmeisl, T. Bligaard, J. Greeley, H. Jónsson and J. K. Nørskov, *Phys. Chem. Chem. Phys.*, 2007, **9**, 3241.
7 J. Rossmeisl, E. Skúlason, M. Björketun, V. Tripkovic and J. Nørskov, *Chem. Phys. Lett.*, 2008, **466**, 68.
8 E. Skúlason, V. Tripkovic, M. E. Björketun, S. Gudmundsdóttir, G. S. Karlberg, J. Rossmeisl, T. Bligaard, H. Jónsson and J. Nørskov, *J. Phys. Chem. C*, 2010, **114**, 18182.
9 V. Tripkovic, M. E. Björketun, E. Skúlason and J. Rossmeisl, *Phys. Rev. B: Condens. Matter Mater. Phys.*, 2011, **84**, 115452.
10 M. E. Björketun, V. Tripkovic, E. Skúlason and J. Rossmeisl, *Catal. Today*, 2013, **202**, 168.
11 C. Lu and R. I. Masel, *J. Phys. Chem. B*, 2001, **105**, 9793.
12 A. Nduwimana, X. G. Gong and X. Q. Wang, *Appl. Surf. Sci.*, 2003, **219**, 129.
13 M. Minca, S. Penner, T. Loerting, A. Menzel, E. Bertel, R. Zucca and J. Redinger, *Top. Catal.*, 2007, **46**, 161.
14 M. Minca, S. Penner, E. Dona, A. Menzel, E. Bertel, V. Brouet and J. Redinger, *New J. Phys.*, 2007, **9**, 386.
15 Z. Zhang, M. Minca, C. Deisl, T. Loerting, A. Menzel and E. Bertel, *Phys. Rev. B: Condens. Matter Mater. Phys.*, 2004, **70**, 121401.
16 J. R. Engstrom, W. Tsai and W. H. Weinberg, *J. Chem. Phys.*, 1987, **87**, 3104.
17 G. Anger, H. F. Berger, M. Luger, S. Feistritzer, A. Winkler and K. D. Rendulic, *Surf. Sci.*, 1989, **219**, L583.
18 C. S. Shern, *Surf. Sci.*, 1992, **264**, 171.
19 E. Kirsten, G. Parschau, W. Stocker and K. H. Rieder, *Surf. Sci. Lett.*, 1990, **231**, L183.
20 S. Gudmundsdóttir, E. Skúlason and H. Jónsson, *Phys. Rev. Lett.*, 2012, **108**, 156101.
21 W. Kohn, *Rev. Mod. Phys.*, 1998, **71**, 1253.
22 G. Kresse and J. Hafner, *Phys. Rev. B: Condens. Matter Mater. Phys.*, 1993, **47**, 558.
23 B. Hammer, L. B. Hansen and J. K. Nørskov, *Phys. Rev. B: Condens. Matter Mater. Phys.*, 1999, **46**, 7413.
24 Dacapo pseudopotential code. URL https://wiki.fysik.dtu.dk/dacapo (Center for Atomic-scale Materials Physics, Technical University of Denmark, Kongens Lyngby, 2011).
25 D. Vanderbilt, *Phys. Rev. B: Condens. Matter Mater. Phys.*, 1990, **41**, 7892.
26 G. Kresse and J. Furthmüller, *Phys. Rev. B: Condens. Matter Mater. Phys.*, 1996, **54**, 11169.
27 H. Jónsson, G. Mills and K. W. Jacobsen, in *Classical and Quantum Dynamics in Condensed Phase Simulations*, ed. B. J. Berne, G. Ciccotti and D. F. Coker, World Scientific, California, 1998, p. 385.
28 G. Henkelman, B. Uberuaga and H. Jónsson, *J. Chem. Phys.*, 2000, **113**, 9901.
29 G. Henkelman and H. Jónsson, *J. Chem. Phys.*, 2000, **113**, 9978.
30 N. M. Marković, B. N. Grgur and P. N. Ross, *J. Phys. Chem. B*, 1997, **101**, 5405.
31 R. Smoluchowski, *Phys. Rev.*, 1941, **60**, 661.
32 R. Bader, *Atoms in Molecules: A Quantum Theory*, Oxford University Press, New York, 1990.
33 G. Henkelman, A. Arnaldsson and H. Jónsson, *Comput. Mater. Sci.*, 2006, **36**, 354.
34 T. C. Leung, C. L. Kao, W. S. Su, Y. J. Feng and C. T. Chan, *Phys. Rev. B: Condens. Matter Mater. Phys.*, 2003, **68**, 195408.
35 T. Bligaard, J. Nørskov, S. Dahl, J. Matthiesen, C. Christensen and J. Sehested, *J. Catal.*, 2004, **224**, 206.
36 G. Kubas, *Metal hydrogen and [sigma]-bond complexes: structure, theory and reactivity*, Kluwer Academic, New York, 2001.
37 F. Yang, Q. Zhang, Y. Liu and S. Chen, *J. Phys. Chem. C*, 2011, **115**, 19311.
38 L. Kristinsdóttir and E. Skúlason, *Surf. Sci.*, 2012, **606**, 1400.
39 M. J. T. C. van der Niet, I. Dominicus, M. T. M. Koper and L. B. F. Juurlink, *Phys. Chem. Chem. Phys.*, 2008, **10**, 7169.
40 M. J. T. C. van der Niet, A. den Dunnen, M. T. M. Koper and L. B. F. Juurlink, *Phys. Rev. Lett.*, 2011, **107**, 146103.
41 M. J. T. C. van der Niet, A. den Dunnen, L. B. F. Juurlink and M. T. M. Koper, *J. Chem. Phys.*, 2010, **132**, 174705.
42 B. Hammer and J. K. Nørskov, *Surf. Sci.*, 1995, **343**, 211.

